Light Scattering and Viscosity Behavior of Dextran in Semidilute Solution

Catalina E. Ioan,[†,‡] Thomas Aberle,[†] and Walther Burchard*[,†]

Institute of Macromolecular Chemistry, University of Freiburg, 79104 Freiburg, Germany; and "P. Poni" Institute of Macromolecular Chemistry, 6600 Iasi, Romania

Received December 7, 1999

ABSTRACT: The solution properties of three dextrans in water with molar masses of 334 000, 506 000 and 2 660 000 g/mol were investigated in a concentration range of 0.1−30%, 0.1−40% and 0.05−65% w/v, respectively. Static and dynamic light scattering, viscometry, and rheological techniques were applied. The forward scattering (at scattering angle $\theta = 0$) could be separated in contributions resulting from repulsive interactions and the true molar mass $M_w(c)$ at concentration c. A similar procedure was applied to the apparent radius of gyration to derive the true radius of gyration $R_g(c)$. A mean field and a scaling approach were applied, and the difference in the results obtained are discussed. Both molecular parameters remained unchanged up to three times the overlap concentration. At higher concentrations a pronounced increase in $M_w(c)$ and $R_g(c)$ indicated association. The high M_w dextran developed a reversible gel point and critical behavior of percolation theory. The time correlation function of dynamic light scattering displayed fast and slow motions where the slow motion was assigned to clusters. Separating the effect of thermodynamic interactions from the mutual diffusion coefficient allowed the self-diffusion coefficient to be obtained, which is governed by hydrodynamic interactions. The range of this interaction was estimated and compared with the cluster size. The zero shear viscosity showed common behavior with a fairly weak increase in the dilute regime and a steep increase at higher concentrations.

1. Introduction

Dextran is the name given to a large class of exocellular bacterial polysaccharides composed of α-D-glucopyronosyl residues, all having preponderant the α(1 → 6) linkage. Some dextrans are composed almost exclusively of the (1 → 6) linkage, whereas others may contain less than 50% of it. The other types of linkages may be (1 → 2), (1 → 3), or (1 → 4), so that a series of α-D-linked D-glucans containing a variety of linkage types is available.[1] Differences in properties are apparently due to the proportion and types of linkage and their arrangement in each dextran molecule. The present study of solution properties in the semidilute to moderately concentrated regime was made with samples prepared by bacteria from *Leuconostoc mesenteroides*, strain B-512(F) type. Dextrans are branched, with 5% degree of branching for the present materials, but it can range up to 33% for other dextrans. Branching occurs mainly in (1 → 3) glycosidic linkages. It still is not clear whether all the branching points are the origin for long chain branching. There are indications that a certain, yet unknown, fraction of the branches are actually merely short side chains.

After similar studies with amylopectin[2] and glycogen[3] with 4.5% and 8% branching points, respectively, it was of interest to investigate another branched glucan. The three polysaccharides belong to the group of hyperbranched materials where a single "focus" functionality A (reducing end group) can exclusively react with one of the B groups in C2, C3, C4, and C6 positions (nonreducing OH groups).[4,5] Dextran resembles amylopectin but here the rather flexible α(1 → 6) bonds establish the chains and the α(1 → 3) bonds the main fraction of branch junctions, while in amylopectin the main chain consists of α(1 → 4) bonds and the α(1 → 6) links form the branching points. A high segment density is a characteristic of branching and has significant influence on the hydrodynamics in dilute solution. It also should influence the mutual interpenetrability of these macromolecules, which becomes detectable in the semidilute and concentrated regime. If an appreciable amount of short chain branches are present, the polymer may behave rather like a sample of lower branching density. The techniques applied in the following are sensitive to long chain branching. Results from static and dynamic light scattering, zero shear viscosity measurements, and oscillatory rheology are presented and combined in a rather comprehensive attempt of interpretation.

2. Theoretical Section

Overlap Concentration. As for linear chains, the overlap concentration represents the most important scaling parameter also for branched macromolecules. This concept was introduced by de Gennes[6] for linear and flexible chains in good solvent to distinguish between dilute and semidilute solutions. In the dilute solution regime the coils are highly swollen, and the mean segmental concentration within a particle is rather low. In this regime, the properties of individual chains can be studied. When a certain concentration c^* is reached, the segments of the coil start to overlap. In the semidilute regime (for $c > c^*$), the segment clouds of the individual chains interpenetrate each other and form a transient network of entangled chains. An important change in behavior is observed when the overlap concentration c^* is exceeded.

The behavior of branched macromolecules differs from that of linear chains. Above c^*, the outer chains of branched macromolecules can penetrate each other in a manner similar to that of linear chains, until the

[†] University of Freiburg.
[‡] "P. Poni" Institute of Macromolecular Chemistry.

10.1021/ma992060z CCC: $20.00
Published on Web 12/16/2000

impenetrable cores start to touch each other. Such an obstruction of impenetrability is caused by the obstacles of the many branching points. A further increase in the concentration will cause either a deswelling of the core or a compression of the swollen structure.

Several definitions were proposed to express the overlap concentration, which can differ up to a factor of 10.[7] We will confine ourselves only to two quantities that are either defined through static, i.e., equilibrium parameters or hydrodynamic quantities, respectively

$$c^*_{A_2} = \frac{1}{A_2 M_w} \propto \frac{M_w}{V_m} \tag{1a}$$

$$c^*_{[\eta]} = \frac{1}{[\eta]} \propto \frac{M_w}{V_m} \tag{1b}$$

where M_w is the weight-average molar mass, A_2 the second virial coefficient, V_m the volume required by the macromolecule, and $[\eta]$ the intrinsic viscosity. Both overlap concentrations are proportional to the ratio of the molecule volume and the corresponding molar mass, but in $c^*_{[\eta]}$, hydrodynamic interactions contribute in addition. The definition of $c^*_{A_2}$ results from thermodynamic (volume) interactions in a good solvent and is appropriate in discussing *static* properties of semidilute solutions.[8] For interpretation of viscosity and rheological data $c^*_{[\eta]}$ is the more adequate parameter.

Static Properties. The static light-scattering (SLS) technique is successfully applied to *dilute solutions* for determining the molecular parameters of individual chains. In semidilute solutions the molecules are not isolated, and strong thermodynamic and hydrodynamic interactions dominate the properties. The light-scattering data are usually analyzed from standard Zimm plots[9] according to the well-known equations

$$\frac{K_c}{R_\theta} = \frac{1}{M_w}\left(1 + \frac{R_g{}^2 q^2}{3} - ...\right) + 2A_2 c + ... \tag{2}$$

with

$$q = \frac{4\pi n_0}{\lambda_0}\sin\left(\frac{\theta}{2}\right) \tag{3}$$

where K is the optical contrast factor, which depends on the difference in the refractive indices of the solution from the solvent, R_θ is the Rayleigh ratio of scattering intensity, λ_0 the wavelength of the used light in a solvent with refractive index n_0, and θ the scattering angle. For branched structures, the Berry plot[10] is more convenient ($(Kc/R_\theta)^{1/2}$ vs $q^2 + kc$), because the often observed curvature of the angular dependence in a Zimm plot becomes largely linearized by the Berry modification. Such plots have two limiting curves, which within experimental error intersect the ordinate in the same point that represents the molar mass, $1/M_w$ or $1/M_w{}^{1/2}$ for Zimm or Berry representations, respectively:

- The scattering curves at zero scattering angle, $\theta = 0$ (forward scattering) give quantitative information on the interparticle interactions, with the second virial coefficient A_2 as its initial part at low concentration.
- The angular dependent scattering data at $c = 0$ is a curve that gives information on the size and shape of the individual macromolecules, parametrized by the radius of gyration R_g.

In the region of semidilute solutions intermolecular interactions exert a considerable influence on the scattering intensity. It is appropriate to consider the forward scattering separately from the angular dependence at finite concentration. The *forward scattering* intensity at zero angle ($R_{\theta=0}$) is caused by concentration fluctuations and is expressed by the relationship[11] $R_{\theta=0}(c) = Kc(RT\partial c/\partial\pi)$ where R is the gas constant, T the absolute temperature, and π the osmotic pressure. Often it is more convenient to use the reciprocal osmotic compressibility $1/RT\ \partial\pi/\partial c$, which may be called the osmotic modulus. Expressing the osmotic pressure in a virial series, one obtains

$$\frac{Kc}{R_{\theta=0}(c)} = \frac{1}{RT}\frac{\partial\pi}{\partial c} = \frac{1}{M_w}[1 + 2A_2 M_w c + 3A_3 M_w c^2 + 4A_4 M_w c^3 + ...] \equiv \frac{1}{M_{app}(c)} \tag{4}$$

where A_2, A_3, etc. are the osmotic virial coefficients. The sum in the brackets comprises the interparticle interactions. The values of the osmotic pressure for various concentrations at zero angle are denoted as reciprocal apparent molar mass ($1/M_{app}(c)$). For dilute solutions the third and higher virial coefficients are negligibly small, but become effective at $c > c^*$. With eq 1a, one can define a scaled concentration

$$A_2 M_w c = \frac{c}{c^*_{A_2}} \equiv X \tag{5}$$

As shown in a previous paper,[12] the higher virial coefficients are related to the second one as follows

$$A_3 M_w c^2 = g_a (A_2 M_w c)^2 = g_a X^2 \tag{6a}$$

$$A_4 M_w c^3 = h_a (A_2 M_w c)^3 = h_a X^3 \tag{6b}$$

where the coefficients g_a, h_a, etc. are structure dependent. In general, we can assume the reduced osmotic modulus being an universal function of X and architecture. Equation 4 then may be rewritten in the scaled form

$$\frac{M_w}{M_{app}(c)} = 1 + 2X + 3g_a X^2 + 4h_a X^3 \tag{7}$$

or alternatively

$$A_2 \frac{R_{\theta=0}(c)}{K} = \frac{X}{1 + 2X + 3g_a X^2 + 4h_a X^3} \tag{8}$$

The dimensionless quantity $M_w/M_{app}(c)$ will in the following be denoted as the reduced osmotic modulus.

The *dimensions* of the particles at zero and finite concentrations may be defined in a formal manner. The initial part of the scattering curve, after extrapolation to zero concentration, is given by the ratio of ($R_g{}^2/3M_w$). Similarly, the corresponding slope of the curves at a *finite* concentration defines an apparent radius of gyration $R_{g,app}(c)$ which is given by the well-known Zimm equation[9] in form of a virial expansion as

$$\frac{Kc}{R_\theta(c)} = \frac{1}{M_{app}(c)}\left(1 + \frac{1}{3}R_{g,app}{}^2(c)q^2 - \cdots\right) = \frac{1}{M_w}\left(1 + \frac{1}{3}R_g{}^2(c)q^2 + 2X + 3g_aX^2 + 4h_aX^3\right) \quad (9)$$

This apparent radius of gyration $R_{g,app}(c)$ is influenced by interparticle interactions. The true radius of gyration $R_g(c)$ at concentration c is found[2a] by comparing the slopes in the two expressions of eq 9.

$$R_g{}^2(c) = R_{g,app}{}^2(c)\cdot\frac{M_w}{M_{app}(c)} \quad (10)$$

This relationship holds as long as no association occurs; i.e., M_w remains unchanged as the concentration is increased. The equations appear to be correct as long as no overlap of coils occurs. At $c \gg c^*$, however, the validity remains not obvious, because in a system of strongly overlapping coils the size of the individual macromolecules no longer can be recognized. This led des Cloizeaux and de Gennes[6] to the conclusion that all measurable quantities should become independent of molar mass. Furthermore, they assumed asymptotic power law behavior at large $X = c/c^* \gg 1$. Thus, eq 7 and eq 10 should be modified and replaced in the asymptotic region of $X \gg 1$ by

$$\frac{1}{RT}\frac{\partial\pi}{\partial c} \rightarrow \frac{1}{M_w}X^p = \frac{1}{M_w}(A_2M_wc)^p = \frac{1}{M_{app}(c)} \quad (7')$$

and

$$R_{g,app}(c) \rightarrow R_gX^{-q} \quad (10')$$

where the arrow indicates asymptotic behavior. The shrinking of dimensions is expected being caused by screening of excluded volume effects due to the interpenetration of the segment clouds. In such an approach, however, the repulsive interaction is neglected. Applying the mentioned two conditions one finds for the exponents

$$p = \frac{1}{1 + a_{A_2}} \quad (11a)$$

$$q = \frac{\nu - \nu_0}{1 + a_{A_2}} = p(\nu - \nu_0) \quad (11b)$$

where a_{A_2} and ν are the exponents in the molar mass dependencies of the second virial coefficient and the radius of gyration ($A_2 \propto M_w{}^{a_{A_2}}$ and $R_g \propto M_w{}^\nu$) and are interrelated via the scaling relationship $\nu = (a_{A_2} + 2)/3$. In the following, we will replace the ν exponent by this relationship for the following reason. In the well-known equation for the asymptotic behavior of the second virial coefficient[13] $A_2 \propto (R_g{}^3/M_w{}^2)$, the ratio of the two quantities depends only weakly on the molecular polydispersity, while the exponent ν obtained from measurements of R_g as a function of M_w strongly depends on the polydispersity ratio M_z/M_w. Furthermore, the molar mass dependence of R_g could be measured only for a restricted number of samples when $R_g > 12$ nm. The virial coefficients, on the other hand, were measured for 13 samples and agreed very satisfactorily with results from 5 samples measured by Nordmeier.[14,15] Thus, the exponent a_{A_2} could be determined with a much higher accuracy than ν. In the concentrated regime a full screening of excluded volume effects may asymptotically be assumed. Under such conditions ν_0 corresponds to the exponent of the unperturbed macromolecules, and eq 10 should pass over to the asymptote

$$R_g{}^2(c) \rightarrow R_{g,app}{}^2(c)X^{2q} = R_{g,app}{}^2(c)\left(\frac{M_w}{M_{app}}\right)^{2(\nu-\nu_0)} \quad (12)$$

But note, full interpenetration can be expected only for flexible linear chains. Equation 12 represents a much weaker increase as given by eq 10 for the dilute regime. Both relationships (eq 7′ and eq 10′) can experimentally be checked. The validity of relation 10 when applied to branched objects is discussed later.

Dynamic Properties. In dynamic light scattering (DLS), a time correlation function (TCF) of the scattering intensity is measured that is formed by an autocorrelator from the scattering intensities measured at a certain starting time $i(q,0)$ and at a very short time interval t later. In normalized form the TCF is given by

$$g_2(q,t) = \frac{\langle i(q,0)i(q,t)\rangle}{\langle i(q,\infty)\rangle^2} \quad (13)$$

where $i(q,\infty)$ is the scattering intensity at very long delay times. For theoretical evaluations mostly the electric field TCF is used $g_1(q,t)$, which is related to the intensity TCF $g_2(q,t)$ by the Siegert relationship.[16] With increasing t, the intensity of the TCF decays to a baseline and can be expressed by a cumulant expansion as given by the equation

$$\ln[g_1(t,q)] = \Gamma_0 - \Gamma_1t + \left(\frac{\Gamma_2}{2!}\right)t^2 - \left(\frac{\Gamma_3}{3!}\right)t^3 + \ldots \quad (14)$$

were the Γ_i are the various cumulants. The first cumulant $\Gamma_1 \equiv \Gamma$ is related to the apparent diffusion coefficient through the relationship

$$\Gamma_1 \equiv \Gamma = q^2D_{app}(q,c) \quad (15)$$

After extrapolation of the data of Γ/q^2 to zero scattering angle, the mutual diffusion coefficient $D(c)$ is obtained, which is related to the z-average translational diffusion coefficient D_z, approximately via the equation[17]

$$D(c) = D_z(1 + k_Dc) \quad (16)$$

The first cumulant corresponds to a characteristic relaxation time τ_0, which is related to the z-average translational diffusion coefficient D_z. According to Stokes−Einstein equation,[18,19] the translational diffusion coefficient at zero concentration depends on the hydrodynamically effective sphere radius R_h

$$D_z = \frac{kT}{6\pi\eta_0R_h} \propto \frac{1}{\tau_0} \quad (17)$$

where k is the Boltzmann constant, T the absolute temperature, and η_0 the solvent viscosity. For increasing particle size, the diffusion slows down and the relaxation time becomes larger.

In semidilute solution, more than one type of motion is often present, and the cumulant procedure becomes a weighted function of the various relaxation processes.

Table 1. Molecular Parameters of Dextrans in Aqueous Solution at 20 °C Where DS Means Dry Substance Content (See also Ref 14)

smpl	DS (%)	$10^{-6}M_w$ (g/mol)	10^4A_2 (mol·mL/g^2)	R_g (nm)	R_h (nm)	$\rho = R_g/R_h$	$[\eta]$ (mL/g)	$c^*_{A_2}$ (g/L)	$c^*_{[\eta]}$ (g/L)
D1	92	2.66	0.54	48	48	1.00	67.79	6.96	14.75
D2	94	0.506	1.76	21	17	1.24	53.14	11.23	18.82
D3	91	0.334	2.02	19	15	1.26	46.07	14.82	21.71

In these cases, the field TCFs can also be approximated by a sum of stretched exponentials, known as Kohlrausch−Williams−Watts function (KWW),[20,21] which often is more convenient and in addition more reliable.

$$g_1(t) = a_1\exp\left[-\left(\frac{t}{b_1}\right)^{\beta_1}\right] + a_2\exp\left[-\left(\frac{t}{b_2}\right)^{\beta_2}\right] + ... \quad (18)$$

with $\sum a_i = 1$ and $0 < \beta_i \leq 1$, where a_i corresponds to the weight of the various processes and b_i and β_i are fit parameters and determine the *mean* relaxation times of individual relaxation processes which are given by

$$\langle\tau_i\rangle = \frac{b}{\beta}\Gamma\left(\frac{1}{\beta}\right) \quad (19)$$

where $\Gamma(x)$ is the gamma function. The exponent β is a measure of the relaxation distribution, small values indicate a broad distribution and $\beta = 1$, monodispersity. The parameter b has the dimension of time.

The mutual diffusion coefficient is influenced by thermodynamic *and* hydrodynamic interactions. According to irreversible thermodynamics,[13,22] one has

$$D(c) = \frac{kT}{f(c)}\left[\frac{M_w}{RT}\frac{\partial\pi}{\partial c}\right] = \frac{kT}{f(c)}\frac{M_w}{M_{app}(c)} \quad (20)$$

where $f(c)$ is the friction coefficient of the diffusing particles at concentration c.

Again some reservations have to be expressed on the validity of eq 20 in the strongly coil overlap region, because the prediction by irreversible thermodynamics was derived so far only for nonoverlapping molecules. In contrast to the treatment of the apparent radius of gyration, no alternative, scaling approach can be offered.

Normalization by $D_z = D(0) = kT/f(0)$ (see eq 15) and multiplication with $M_{app}(c)/M_w$ leads to

$$\frac{D(c)}{D(0)}\frac{M_{app}(c)}{M_w} = \frac{D_{self}(c)}{D(0)} = \frac{f(0)}{f(c)} \quad (21)$$

where $D_{self}(c)$ is the self-diffusion coefficient at concentration c that no longer depends on the thermodynamic interaction, but still depends strongly on c because of increasing friction. At zero concentration, the Stokes equation $f(0) = 6\pi\eta_0 R_h$ can be applied, where R_h is the hydrodynamic radius of the particles. The concentration dependence of the frictional coefficient is not known. Only at very dilute solutions can a linear relationship be assumed, but otherwise $f(c)$ depends nonlinearly on concentration and the shape of the macromolecule. For symmetry reasons, we split off the factor $6\pi\eta_0$ also from $f(c)$ and obtain

$$\frac{f(c)}{f(0)} \equiv \frac{R_h(c)}{R_h} \quad (22)$$

This formally defined $R_h(c)$ is actually no particle radius but rather a correlation length that describes a long-range effect of frictional interaction among the particles. Equations 20−22 hold as long as no association of macromolecules takes place; i.e., if attractive interactions are not effective. The influence of association will be considered later in due course.

3. Experimental Section

Samples and Solution Preparation. Three dextran, products of Sigma, briefly denoted as D1, D2, and D3, with different molecular weights of $M_w = 2.66 \times 10^6$, 506 000, and 334 000, respectively,[14] were analyzed. Measurements were carried out at 20 °C. Water with 0.01% sodium azide (NaN_3) added was used as solvent. The samples have been directly dissolved to obtain the concentration ranges: 0.05−40% for D1, 0.1−40% for D2, and 0.1−30% for D3. For D1, some high concentrations were obtained by evaporation. From a stock solution of 40%, concentrations up to 65% were obtained, and from the 15% stock solution, concentrations up to 52.2% were possible. The dilute region was used to obtain the molecular parameters, which are given in Table 1. Until 20%, dust free solutions were prepared by using 0.2 μm filters; for higher concentrations 5 μm filters were used.

Dry substance (DS) content was determined in a moisture analyzer (Sartorius MA 40). The obtained values scattered around 92%.

Static Light Scattering (SLS). Measurements were made with a fully computerized and modified SOFICA photogoniometer (G. Baur, Instrumentenbau, Hausen, Germany), that was equipped with a 2 mW HeNe laser ($\lambda_0 = 632.8$ nm). An angular range from 35 to 145°, in steps of 5° was covered. The refractive index increment $dn/dc = 0.151$ mL/g was taken from the literature.

Dynamic Light Scattering (DLS). Measurements were performed using an ALV photogoniometer (ALV, Langen, Germany) equipped with an ALV 5000 correlator. A Spectra Physics krypton ion laser ($\lambda_0 = 647.1$ nm) served as light source. Measurements were made in an angular range from 30 to 150°, in steps of 10°.

Viscosity. For fairly diluted solutions an automatic Ubbelohde viscometer (Schott, Germany) with a capillary of 0.63 mm in diameter was used. At higher concentrations a CS-Bohlin rheometer, with a 4 cm/1° cone and plate shear geometry was used, and the viscosities were checked for a possible shear gradient dependence. The shear gradient was controlled by the rheometer in the range 10^{-2}−10^3 s^{-1}, which corresponded to the stress range from 0.06 to 40 Pa.

4. Results

Molecular Parameters from Dilute Solutions. Three dextrans, D1, D2, and D3, of different molar masses were measured by SLS and DLS in aqueous solutions in concentration ranges of 0.05−0.5% for D1 and 0.1−1% for D2 and D3 at 20 °C. A full characterization of 14 samples in the dilute regime is found in ref 14. Viscosity measurements were performed in the concentration range of 1−5%. Figure 1 shows as an example the Berry plot for D1 in water with 0.01% NaN_3, for the whole concentration range. The dilute solution range (inset in Figure 1) led to the evaluation of molar mass M_w, the second virial coefficient A_2, and the radius of gyration R_g. The molecular parameters for the three investigated samples are given in Table 1

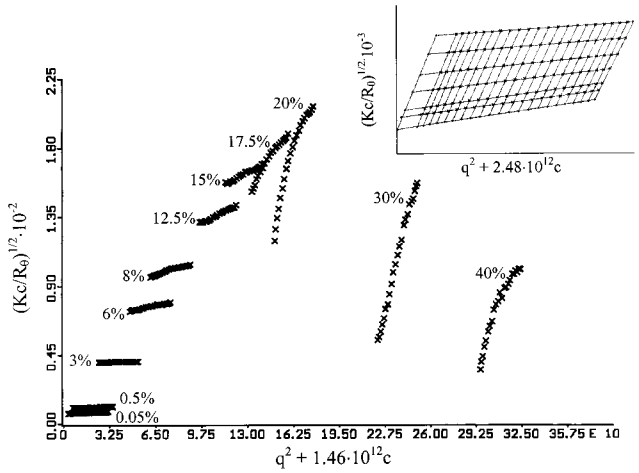

Figure 1. Berry plot of static light-scattering intensities from dextran D1 in water. Concentration range: 0.05% ≤ c ≤ 40% (w/v). Inset: dilute behavior (c ≤ 0.5%). $M_w = 2.66 \times 10^6$ g/mol; $R_g = 48$ nm, $A_2 = 5.4 \times 10^{-5}$ mol mL/g^2.

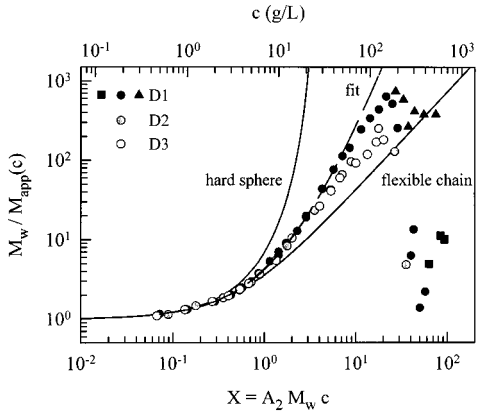

Figure 2. Plot of $M_w/M_{app}(c)$ against the scaled concentration $X \equiv A_2M_wc \equiv c/c^*_{A_2}$. The full lines represent the theoretical curves for hard spheres[30] and flexible linear chains.[31] The dashed line represents a curve obtained according to eq 7 with the three dextran samples, before the onset of a turnover. The data points represented by circles refer to experiment and were obtained by dilution of different stock solutions. In the case of D1, two additional sets of data are shown, one represented by ■ was obtained by evaporation of a stock solution with a concentration of 400 g/L, and another (▲) was obtained by evaporation of the stock solution with a concentration of 150 g/L. The data from D1 are also plotted as a function of c.

together with the data from dynamic LS and capillary viscometry.

Static Light Scattering from Samples in the Semidilute Regime. The measurements were performed with the computerized setup described in the Experimental Section. Suitable programs facilitated the evaluation. Figure 1 shows the Berry plot for D1 for the whole concentration range. In the dilute concentration regime, a low angular dependence and a linear concentration dependence were found. With increasing concentration, the transition to the semidilute regime occurs. The concentration dependence is no longer linear but develops a significant upturn. A pronounced angular dependence becomes noticeable. At even larger concentrations, the concentration dependence at zero scattering angle passes through a maximum and then decreases again. The points at zero scattering angle for each concentration were taken as reciprocal apparent molar masses. The apparent molar masses $M_{app}(c)$ are concentration dependent. Similarly, the slopes were taken as a measure of apparent radius of gyration $R_{g,app}(c)$ at this concentration c.

In Figure 2 the reduced osmotic modulus $M_w/M_{app}(c)$ for all three samples is plotted against the normalized concentration $X = c/c^*_{A_2} = A_2M_wc$. The figure also contains theoretical curves predicted for hard spheres and for flexible linear chains. Until a certain concentration the points for the three investigated dextran samples follow one common *master curve*, which can be described by eq 7. At about three times the overlap concentration the points for the three samples begin to deviate from each other. A drastic change in behavior occurs at about $X \cong 20$, where a strong downturn indicates association.

Further experiments at large X showed that we had to take care of how a certain concentration was prepared. In one case, the samples were directly dissolved; in the second one, a lower concentration was prepared, and the corresponding higher concentrations were obtained by water evaporation. For systems in thermodynamic equilibrium both procedures should give the same result for the light-scattering data. However, a different result is obtained for associating systems showing hysteresis. We checked this question with a concentration of 15%, the point just where a downturn of $M_w/M_{app}(c)$ occurs. Six larger concentrations were prepared (▲). For the first three points, we obtained within experimental error almost the same result, but for the last three points, no coincidence was found. This probably is caused by the above-mentioned hysteresis or by bacterial degradation. The first reason is supported by the findings with the 65% solution that was prepared by water evaporation of a 40% solution (■). Here a difference by a factor of 10 was observed. The observed hysteresis, of course, reduces reproducibility (20% error). Bacterial degradation with the 15% solution could not be excluded, because the sample had been kept for about 1 month. In the case of the 40% solution, we received evidence for a gel state that was checked by rheology (see below). The oscillatory measurements were made only up to 40%, because the amount of sample became too low after evaporation, and the cone−plate cell could not be filled.

The analysis of the fit curves in terms of the virial coefficients was better done in a plot of the normalized forward scattering $R_{\theta=0}A_2/K$ vs X (not shown but see eq 8),which has a characteristic maximum, and led to the following values of the coefficients $g_A = 0.354$ and $h_A = 0.036$. The change in behavior, when entering the semidilute regime, is also demonstrated by the ratio of the apparent mean square radius of gyration to the true mean square radius of gyration $(R_{g,app}(c)/R_g)^2$. Figure 3 shows these data as a function of X. The figure contains also a theoretical straight line that will be discussed later.

Dynamic Light Scattering. At low concentrations, up to 10%, only one mode is observed, which is close to a single exponential (Figure 4a). At higher concentrations a second mode becomes noticeable that increases in magnitude with increasing concentration and simultaneously is strongly slowed. In the low concentration region, no angular dependence is observed. At high concentrations, both the slow and the fast motions show angular dependencies as shown in Figure 4b. The strong angular dependence of the slow motion indicates the presence of large particles. A detailed analyses is postponed to the discussion.

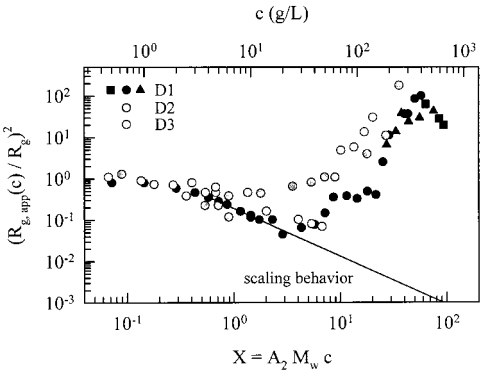

Figure 3. Ratio of the apparent to the true mean square radius of gyration $(R_{g,app}(c)/R_g)^2$ plotted as a function of X. The upper scale is the concentration for D1. The straight line corresponds to the scaling prediction according to eqs 11b and 26. The exponent is $2q = -1.16$.

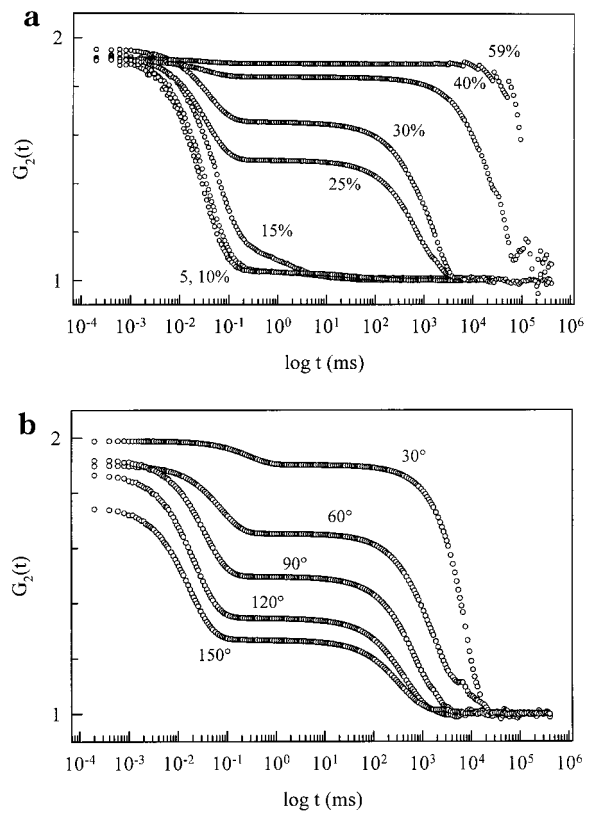

Figure 4. (a) Concentration dependence of time correlation functions at 90° of D1 solutions. (b) Angular dependence of time correlation functions in dynamic light scattering from a 30% D1 solution. Fast and slow modes of motion are clearly recognized.

Viscosity. The viscosity was measured in the dilute regime in an Ubbelohde viscometer with a capillary of 0.63 mm in diameter using the automatic instrument of Schott. For concentrations higher than 5% measurements were made in a CS−Bohlin rheometer. For each of these concentrations the shear rate dependence was measured. No shear dependence was observed up to 25% solutions. At 30% a small shear thinning is first observed which merged in a shear independent plateau for higher shear gradients. Special behavior was observed for the 40% solution, which displayed first shear thickening that beyond 0.2 s^{-1} is followed by shear thinning. This shear thinning not necessarily means destruction of the physical network. Rather it indicates sliding of associated chains. Note: A physical network contains no fixed permanent cross-links. Higher concentrations could be not measured because of lack of substance. In Figure 5 the zero shear specific viscosity is plotted against $c[\eta]$ in a double logarithmic scale. The plot shows common behavior with a weak increase in the dilute region and a very steep increase in the higher concentrated regime. The asymptotic slope corresponds to power law behavior with an exponent of 4.92. A slight variation in behavior for the three different samples is observed, but all curves merge into the same power law at higher concentrations. For comparison Figure 5 also contains data from glycogen[3] and amylopectin.[2]

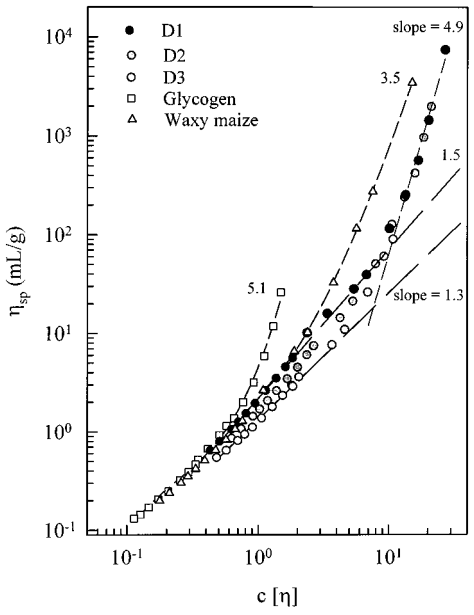

Figure 5. Dependence of the zero shear specific viscosity η_{sp} of dextran samples as a function of $c[\eta]$, where $[\eta]$ is the intrinsic viscosity. The fairly dilute solutions were measured with an Ubbelohde viscometer, whereas for higher concentrations the use of a stress-controlled rheometer was required. The plot also contains the data from two other hyperbranched polysaccharides, glycogen[3] and amylopectin,[2] of different branching densities (8% and 4%, respectively).

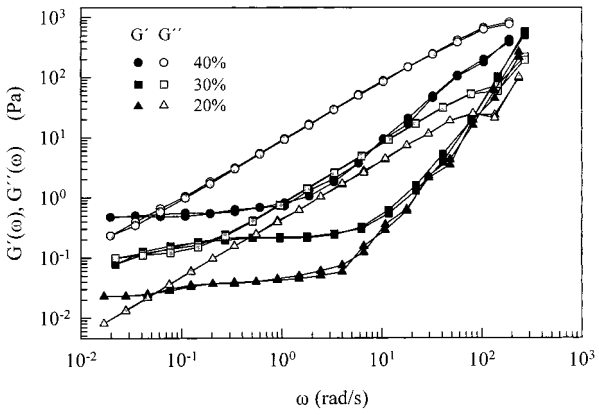

Figure 6. Elastic $G'(\omega)$ and loss $G''(\omega)$ moduli as a function of frequency for D1 at three different concentrations. The plateau at low frequencies gives indication to the elastic modulus of a weak gel.

For the high concentrations, we also measured the elastic and loss moduli by oscillatory rheology. The results are plotted in Figure 6. At low frequencies a plateau is formed for $G'(\omega)$ that may correspond to the elastic modulus of a gel, but the loss modulus still remains larger than the elastic one. Measurements at such high concentrations are difficult to perform, be-

cause a weak evaporation of water may induce a significant influence on the behavior for a system near the gel point. Below a concentration of 20%, such a plateau was not longer observable. The concentration dependence will be discussed later.

5. Discussion

True Molar Mass $M_w(c)$ at Concentration c. For nonassociating polymers, the apparent molecular mass decreases with the concentration as indicated by eq 4. The corresponding osmotic modulus $M_w/M_{app}(c)$ increases. In a plot of these data against the reduced concentration $X = A_2M_wc$, a common curve, at least up to $X = 3$, is obtained for all three samples. Deviation from this curve (shown as dashed line in Figure 2) occurs at lower X, when M_w is small and at much higher X values for the high molar mass sample. Therefore, the dashed line may be considered as a master curve that describes the scaled repulsion among the particles.

The deviations from this master curve can be interpreted as an increase of the molar mass due to association. In such a case eq 4 has to be modified as follows

$$\frac{Kc}{R_{\theta=0}(c)} = \frac{1}{RT}\frac{\partial\pi}{\partial c} = \frac{1}{M_w(c)}[1 + 2A_2M_w(c)c + 3A_3M_w(c)c^2 + 4A_4M_w(c)c^3 + ...] = \frac{1}{M_{app}(c)} \quad (4')$$

We now formed the ratio of the master curve to the measured osmotic modulus, which is the ratio of eq 4/eq 4′. When this is multiplied with the molar mass M_w at zero concentration we obtain

$$\frac{M_{app,exp}(c)}{M_{app,master}(c)} = \frac{M_w(c)[1 + 2A_2M_wc + 3A_3M_wc^2 + 4A_4M_wc^3 + ...]}{M_w[1 + 2A_2M_w(c) + 3A_3M_w(c)c^2 + 4A_4M_w(c)c^3 + ...]} \cong \frac{M_w(c)}{M_w} \quad (23)$$

The right side of this equation is obtained under the assumption that the repulsions between nonassociated and associated particles are not very much different from each other; i.e., the increase in $M_{app,exp}(c)$ is fully attributed to the increase of the true cluster molar mass at concentration c. This approximation is exact for spherical particles, because for such structure one has $A_2M_wc \propto M^0$ and the repulsion effect remains unchanged when larger spheres (or densely packed clusters with $d_f = 3$) are formed on aggregation. The approximation becomes increasingly worse for structures with a lower fractal dimension d_f. However, even on random association of linear chains, the fractal dimension increases from $d_f = 1.7$ toward $d_f = 2.5$, which in turn improves our intuitive approximation. For branched samples the fractal dimension is with $d_f > 2.2$ already closer to $d_f = 3$. No quantitative estimation of the quality of this approximation could yet be made. We are aware of the speculative character of the approach in eq 23.

The thus calculated true molar mass remains almost unchanged up to a concentration of about 60 g/L ($X \cong 10$). Then a steep increase of the molar mass occurs with the concentration. Figure 7 shows the effect of correction for the repulsion, where the reciprocal molar masses are

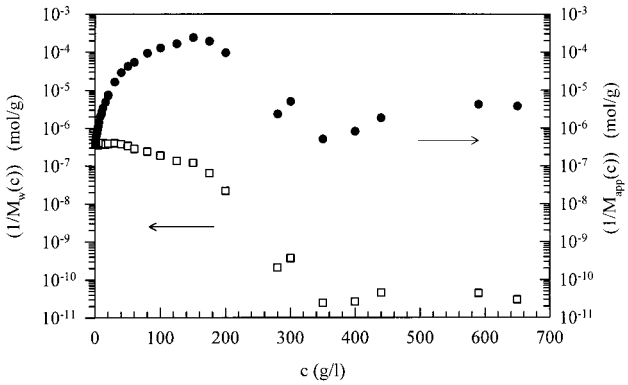

Figure 7. Concentration dependence of the reciprocal molar masses for D1: (●) $1/M_{app}(c)$ and (□) $1/M_w(c)$ corrected for the effect of repulsion, according to eq 23.

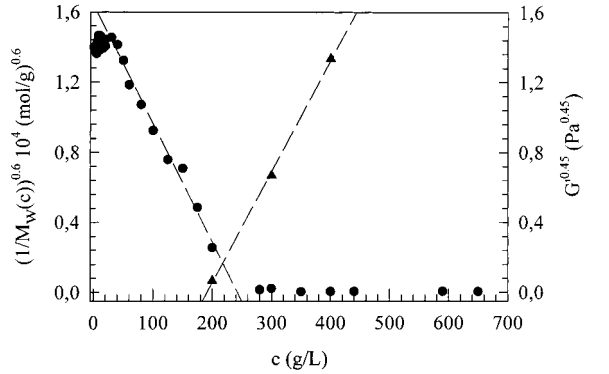

Figure 8. Estimation of the gel point for D1, by plotting $(1/M_w(c))^{0.6}$ and $G'(\omega)^{0.45}$ against the concentration. The exponents were chosen to minimize deviations from the straight lines.

plotted. Apparently the reciprocal true molar mass approaches a value of zero, or in other words, the molar mass increases beyond all limits. This is a characteristic of gelation. To check the correct value of the gel point, we plotted in Figure 8 $(1/M_w(c))^{0.6}$ against concentration c. The exponent was chosen to minimize the deviations from the straight line. In this plot the point of gelation occurs at a concentration $c_{cr} = 240$ g/L. Beyond this concentration, gel behavior is observed. In oscillatory rheology, a plateau value was observed at low frequencies corresponding to an elastic modulus $G'(\omega)$ (Figure 6). This plateau value may tentatively be considered as the elastic modulus of a weak gel, because in a wide frequency range the loss modulus still remained larger than the elastic one (see also the comment at the end of section 4.). The concentration dependence of these moduli is also plotted in Figure 8. Accordingly a zero elastic modulus would be reached around 200 g/L to be expected for particles dissociating into subcritical clusters. However, the clusters in the pregel will have already a certain elastic modulus, and this might be the reason the gel point seems to occur at lower concentration.

Critical Behavior. Next the critical behavior may be examined. To this end the concentration dependent molar mass $M_w(c)$ is plotted against $c_{cr} - c$ on a double logarithmic scale (Figure 9), where c_{cr} is the critical gel concentration and c the actual concentration. This plot sensitively depends on the gel point. Theories predict power law behavior of the form

$$M_w(c) \propto (c_{cr} - c)^y \quad (24)$$

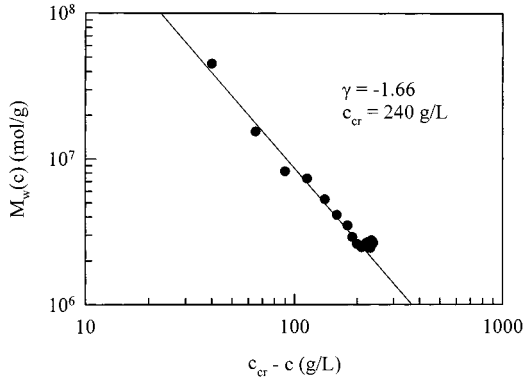

Figure 9. Concentration dependent molar mass $M_w(c)$ of D1 as a function of $(c_{cr} - c)$, where c_{cr} is the critical concentration and c the actual concentration. The exponent $\gamma = -1.66$ indicates the validity of percolation prediction.[25]

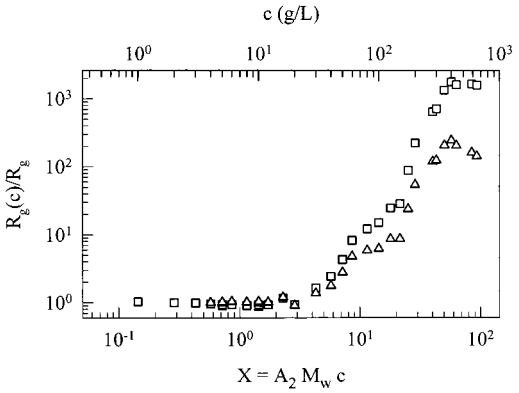

Figure 10. Concentration dependence of the D1 dimensions corrected for repulsions, according to eqs 10 and 23 (□) (apparent virial approach) and according to eq 27 (△) (scaling approach).

A value of $\gamma = -1.78$ is predicted by percolation theory,[25] whereas the mean field theory by Flory[4] and Stockmayer[26] predicts $\gamma = -1.0$. For the critical point of $c_{cr} = 240$ g/L, the exponent $\gamma_{exp} = 1.66$ is clearly in the range of the percolation theory. The somewhat lower value than that of the percolation theory may be well in the range of the experimental error. So far as is known to us, this is the third example[27] where critical behavior of reversible gelling systems was found. In all cases the data were much closer to percolation than to mean field theory.

One consequence of the validity for percolation theory would be that the elastic modulus should increase with an exponent μ_{el}

$$G' \propto (c_{cr} - c)^{\mu_{el}} \tag{25}$$

with $\mu_{el} = 2.2$.[28] The exponent chosen in Figure 8 just meets this conditions and should result in a linear relationship. However, the critical point would now lie at a lower concentration than for $M_w(c)$. The low number of experimental points admits no reliable check.

Concentration Dependence of Dimensions. In Figure 3 the apparent mean square radius of gyration $R_{g,app}^2(c)$ at concentration c, normalized by the mean square radius of gyration R_g^2 at zero concentration, is plotted against the parameter X. This apparent radius of gyration corresponds to the experimentally observed initial slope in the Berry plot. In the following, we will discuss only the curve for the highest M_w (filled symbols in Figure 3). Up to three times the overlap concentration, one observes a decrease by a factor of 20 and then a marked increase of the dimension, that at about $X \cong 70$ passes through a maximum and then decreases again. The initial decrease corresponds to the thermodynamically expected screening of interparticle interactions. As was shown previously,[3] this effect of the interaction may be corrected by applying eq 10, which is correct in the dilute regime. No change in the dimension is obtained up to $X = 3$ (i.e., $c = 20\%$). The steep increase that follows is a clear indication for cluster formation. The effect of the correction with eq 10 is seen in Figure 10.

As was already mentioned, the validity of eq 10 remains questionable in the region of $c \gg c^*$. The scaling assumption of eqs 7′ and 10′ may here be more reasonable. This would give asymptotically a decrease of the apparent radius of gyration in form of a power law as given by eq 11b; i.e., $q = (\nu - \nu_0)/(1 - a_{A_2})$. For linear chains all exponents are known, but for branched samples the value of the exponent ν_0 may be a point of discussion. If we interpret the "unperturbed" dimensions as those where the volume of the repeat units has no influence, then the result obtained by Zimm and Stockmayer[29] can be used, which is $\nu_0 = 0.25$. Inserting the experimental value of $\nu = 0.447$ and $a_{A_2} = -0.66$, one obtains $q = 0.580$. The solid line in Figure 3 corresponds to a fit of

$$\frac{R_{g,app}^2(c)}{R_g^2} = 0.19X^{-1.16} \tag{26}$$

which represents the experimental data very satisfactorily up to the point where the sudden increase of $R_{g,app}(c)$ occurs. In addition to the comment to eq 10′ an exponent of $\nu = 0.25$ would correspond to a fractal dimension of $d_f = 4.0$ which appears physically not to be feasible. The derived exponent $q = 0.58$ that surprisingly well describes the experimental data may be accidental. However, we should emphasize that the limits of hard spheres ($q_{sphere} = 0$) and linear flexible chains ($q_{chain} = 0.115$) are correctly recovered. Moreover, we found also good agreement with experimental data for amylopectin with $\nu_0 = 0.25$. This coincidence appears to us not to be fully accidental, but before a consistent theory has been developed, we have to consider eq 10′ only as a guideline for a suitable but empirical fit.

Similar to what was done for the calculation of $M_w(c)/M_w$, we now assume

$$\frac{R_g(c)}{R_g} \cong \frac{R_{app,exp}(c)}{R_{app,master}(c)} \tag{27}$$

The result is shown in Figure 10, with Δ as symbols. Up to values of $X = 8$ a remarkably good agreement is obtained with the apparent virial approach of eq 10, according to the Debye approximation. In the asymptotic regime, however, ($X > 8$) a much weaker increase is found. We also checked the curve of eq 7 for the reduced osmotic modulus with the scaling law, which is shown in Figure 13. Our fit curve very nicely approached the asymptotic scaling slope which, however, is reached in the region of $X > 20$. Indeed, eq 7′ appears to be valid for every architecture if the correct fractal dimension is used. A fit of the osmotic modulus with a virial expansion remains exact for hard spheres,[30] because a region of coil interpenetration ($c > c^*$) can never be

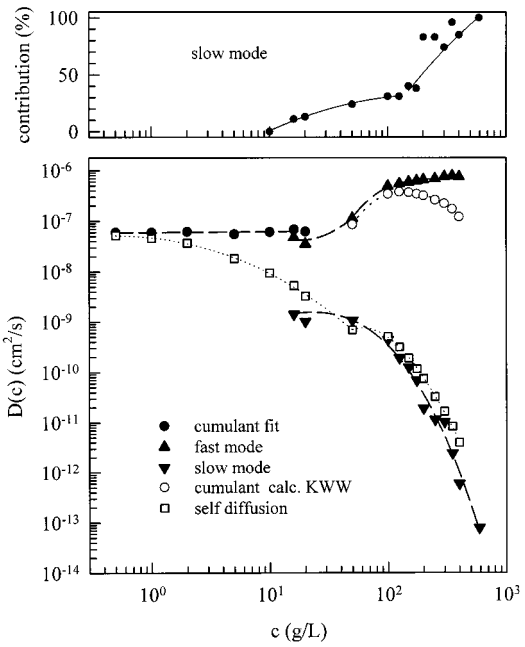

Figure 11. Mutual diffusion coefficients $D(c)$ as a function of concentration for D1. The filled circles refer to the cumulant fit. The different curves correspond to the fast (triangle up) and slow (triangle down) modes of translational motions, resulting from a KWW analysis of the time correlation functions. The open circles represent the cumulative diffusion coefficient obtained from the sum of the two modes. The self-diffusion coefficients, obtained according to eqs 20 and 21, are plotted as open squares. Upper part of Figure 11: Contribution in percent of the slow mode with increasing concentration.

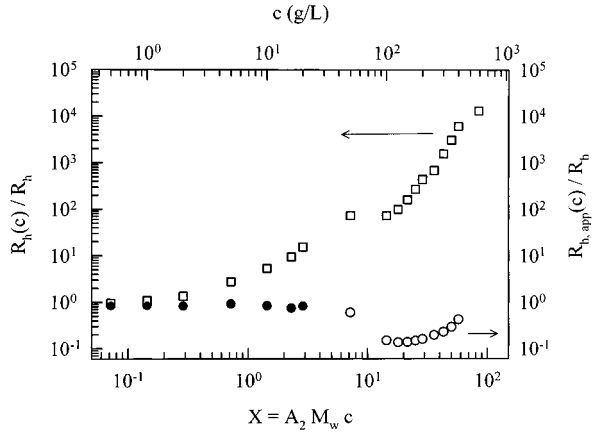

Figure 12. Concentration dependence of $R_h(c)/R_h$ (eq 22) after correction for repulsive interactions. The symbols are the same as in Figure 11.

entered. The virial expansion loses more and more its range of validity with increasing coil interpenetration, and for full coil−coil interpenetration, the renormalization group theory with its scaling asymptote becomes applicable over almost the whole range of semidilute concentrations.[31,32] For our branched samples, the apparent virial fit remained valid for the reduced osmotic modulus over the whole experimentally investigated range and correctly describes the full crossover from nonscaling to scaling behavior.

Good agreement between the apparent virial and scaling approaches was found also for the apparent radius of gyration if $X < 8$. Beyond $X = 8$, however, significant deviations are obtained. This is seen in Figure 10 when a correction for the repulsive interaction was applied. This correction is not fully correct for

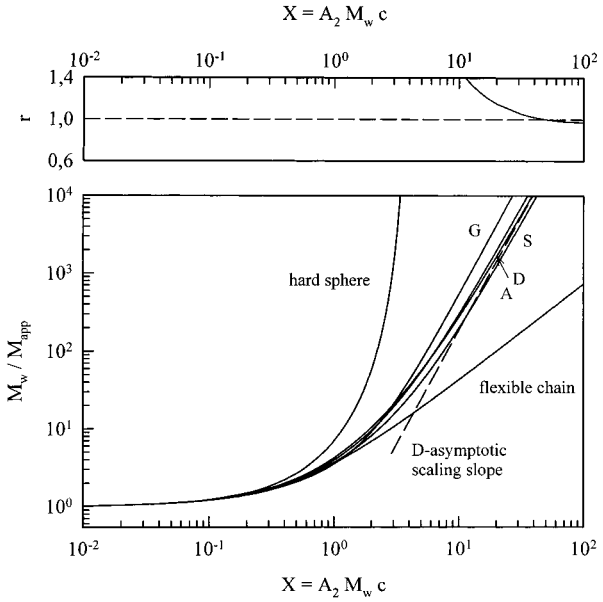

Figure 13. Osmotic modulus master curves for polymers of the same chemical structure but different branching densities (8% glycogen (G); 4% degraded starches (S), amylopctin (A), and dextran (D). The graphs demonstrate the influence of branching. The slope of the straight line at large X values is that predicted by scaling arguments given by eq 7′.

associated molecules, because of the effect of attractive forces due to the attached stickers[32] (here in form of OH groups which can form hydrogen bonds). These stickers slightly decrease the free energy of interaction, but in a first approximation it causes only a certain decrease in the second virial coefficient. As long as the higher virial coefficients can be expressed in terms of the second one, everything remains as displayed so far. However, close to the point of gelation the higher virial terms may have a significant contribution[33] that will be examined in a forthcoming treatment. In our experiments we still assumed unique dependence on X alone, also for the associated clusters. Within this assumption, we may state that the correct increase should lie between the upper limit for impenetrable particles and the lower limit for fully penetrable coils.

For a critical system also the dimensions should diverge at the gel point. Here again the critical behavior is given by a power law if percolation remains valid. Because of the yet not fully clarified correct estimation of the true dimensions, we did not apply this check.

Concentration Dependence of Friction. The TCF's in Figure 4 displayed only a single exponential diffusion mode at small concentrations, but at higher concentrations ($X > 4$), a slow mode occurs in addition. This quickly increased in weight and correlation time when the concentration was increased. Up to a concentration of about 20 g/L, the common cumulant fit could be made for the determination of the mutual diffusion coefficient. Such a fit was no longer accurately possible when the slow motion appeared. In these cases, the TCF's were fitted by the Kohlrausch−Williams−Watts[20,21] procedure which uses stretched exponentials. The fit was made according to eq 18, and the data are plotted in Figure 11. The diffusion coefficient of the fast motion increases weakly as expected, but the diffusion coefficient of the slow motion decreases enormously by 4 decades. From these two diffusion coefficients and the fractions of fast and slow modes, the cumulative diffusion coefficient was calculated by the weighted sum of

the two separately determined components. This procedure gives the data of the open circles in Figure 11, where for the slow diffusion coefficient we have used the smoothed data.

These data from dynamic light scattering could be handled as described by eqs 20 and 21, with the modification that for associating particles the constant molar mass M_w has to be replaced by the corresponding mass $M_w(c)$ at concentration c. The nonnormalized self-diffusion coefficient is plotted as open squares in Figure 11. To our surprise, the curve of self-diffusion at high concentrations agreed almost completely with the diffusion of the slow particle. This means that the motion is fully governed by the size of the large particles.

In Figure 12, $R_h(c)/R_h$ is plotted against X, which is given by eqs 20−22. The quantity $R_h(c)$ is actually no radius but rather a correlation length for the hydrodynamic interaction, i.e., the range where a change in a position r_1 has still a noticeable influence in a position r_2. This interaction range is apparently much larger than the cluster size. Comparison of Figure 10 with Figure 12 shows that this interaction radius is at the highest concentration about 5−10 times larger than the cluster radius.

Zero Shear Viscosity. Only a few comments will be made on this property. Figure 5 is of interest, because it shows the influence of branching density. Glycogen has the highest branching density and was shown to behave similar to spherelike particles.[3] It follows waxy maize with about 4−5% branching points and finally the dextrans. Apparently the asymptotic steep increase is shifted to larger values of $c[\eta]$ when the branching density decreases. It would be of interest to compare this with the linear α(1 → 6) and α(1 → 4) glucans. Unfortunately, linear dextran was not available to us, and amylose, the corresponding linear α(1 → 4) glucan, is not stable in aqueous solution and crystallizes at room-temperature already below 0.5% (w/v). The same tendency has already been observed with the molar mass dependence of dilute viscosities, where the dextrans show the highest values for the intrinsic viscosity $[\eta]$, followed by amylopectin and levan and finally glycogen.[22] From the plot of the zero shear viscosity in Figure 5 we can draw the conclusion that the $c[\eta]$ dependence appears to be the same for different molar masses of the same architecture, but it is certainly not universal with regard to different molecule architectures. After finishing the experimental work, we came across a recent paper by Durrani and Donald,[24] who found for two amylopectins of much lower molar masses a relationship that nicely agrees with our curve in Figure 5. However, no indication for association was found. This finding is not in disagreement with the static and dynamic light-scattering results, because in light scattering mainly the large objects contribute, whereas the zero shear viscosity is rather insensitive to a few large particles in the solution.

6. Conclusion

The present experiments showed some special properties, which may be summarized as follows.

1. Universal behavior is found only up to a certain overlap concentration ($c/c^* < 4$). The range of validity depends on the molar mass. The onset of deviation is shifted to higher concentrations as the molar mass M_w increases. The master curve differs slightly for different branched glucans. This is shown in Figure 13. Glycogen and amylopectin are identically in chemical structure and vary only in the branching density. The α(1 → 6) bond in dextran is more flexible than the α(1 → 4) links in glycogen and amylopectin, but this difference in flexibility has only little effect.

2. Deviations from universal master curves indicate association. With the aid of the master curve, it was possible to split off the interaction from the apparent molar mass that admitted estimation of the true molar mass at concentration c. The molar mass increased for the highest dextran sample beyond all limits at a certain concentration. Taking this critical concentration as point of reversible gelation, critical behavior was found, which with the exponent of 1.6 is much closer to the percolation prediction than to mean field theory by Flory and Stockmayer. Beyond the critical concentration, an extended plateau of the elastic modulus develops.

3. The apparent radius of gyration is also influenced by the thermodynamic interaction. The applied estimation placed the data between of upper and lower limits, defined by no and full segment cloud interpenetration, respectively. The influence of repulsion could be split off in both approaches such that the true dimensions from the molecules and clusters at concentration c could be determined. The dimension remained unchanged up to the concentration where deviations in the molar mass from the master curve were observed. Large clusters are formed at larger concentrations.

4. A slow mode of motion becomes noticeable at the same concentration at which the molecules grow in size. In this region, the different coefficients from the slow and fast motion were determined. The slow motion did not significantly contribute to the average diffusion coefficient.

Structure determination of polymers in semidilute solution is generally considered as being impossible. This conclusion was mainly drawn from viewing the structures in real space, for instance by electron microscopy. At least for linear flexible chains the various macromolecules are indistinguishable, and the structure observed cannot be assigned to a special macromolecule or aggregated particle. On the other hand, this paper and earlier ones demonstrate that different architectures can be distinguished by light scattering, if the overlap concentration is used as scaling parameter. This became possible via measurement of the *interaction* among the particles in solution, because the repulsive volume interaction is strongly dependent on the particle architecture. Once this interaction is known, it can be used for determining the true molar mass of particles at finite concentration, and this holds even for semidilute concentrations. The evaluation of true particle dimensions is more involved, but combining the dimensions of the individual particles at zero concentration with the free energy of interaction a rough estimation of the dimension in the overlap regime can be made within upper and lower limits. Both limits can only be estimates when partial interpenetration of segment clouds takes place. The repulsion among aggregated particles increases slightly when the fractal dimension d_f of the molecules and of the particles is smaller than 3.0 (compare with eq 23). It also changes its value, but in the opposite direction, when shrinking occurs by which the fractal dimension d_f of the aggregates increases. This partially compensates the first process. In the alternative treatment the choice of ν_0 and the neglect of interaction *among* the particles is a question-

able assumption. The applied techniques will be further refined in a treatment that presently is in work.

Finally we wish to emphasize the pragmatic character of our approach to this intriguing problem of semidilute solutions. We simply used known relationships whose limits of applicability are not yet well explored, in particular when branched or only partially penetrable particles are considered. Our suggestions may be taken as an invitation to theoreticians to derive a well-founded theory based on measurable quantities.

Acknowledgment. C.E.I and W.B. thankthe Romanian Academy in Iasi and the Deutsche Forschungsgemeinschaft for a 3 months grant given within a special agreement among both committees. W.B. benefited greatly from a significant discussion with Professor Michael Rubinstein, University of North Carolina, and Dr. Jack Douglas, at NIST.

References and Notes

(1) (a) Sandford, P. A.; Baird, J. Industrial Utilization of Polysaccharides. In *The Polysaccharides*; Aspinall, G. O., Ed.; Academic Press: San Diego, CA, 1983; Vol. 2, p 474. (b) Kenne, L.; Lindberg, B. Bacterial Polysaccharides. In *The Polysaccharides*; Aspinall, G. O., Ed.; Academic Press: San Diego, CA, 1983; Vol. 2, p 346.
(2) (a) Aberle, T.; Burchard, W. *Starch* **1997**, *49*, 215. (b) *Comput. Theor. Polym. Sci.* **1997**, *7*, 215.
(3) Ioan, C. E.; Aberle, T.; Burchard, W. *Macromolecules* **1999**, *32*, 8655.
(4) Flory, P. J. *Principle of Polymer Chemistry*; Cornell University Press: Ithaca, NY, 1953.
(5) Erlander, S.; French, D. *J. Polym. Sci.* **1956**, *20*, 7.
(6) De Gennes, P.-G. *Scaling Concepts in Polymer Physics*; Cornell University Press: Ithaca, NY, 1979.
(7) Burchard, W. *Makromol. Chem., Macromol. Symp.* **1988**, *18*, 1.
(8) Freed, K. F. *Renormalization Group Theory of Macromolecules*; Wiley: New York, 1987.
(9) Zimm, B. H. *Chem. Phys.* **1948**, *16*, 1093.
(10) (a) Berry, G. J. *J. Chem. Phys.* **1966**, *44*, 4550. (b) Burchard, W. *Adv. Polym. Sci.* **1983**, *48*, 1.
(11) (a) McQuarrie, D. A. *Statistical Mechanics*; Harper & Row: New York, and Evanston, IL, 1976. (b) Friedman, A. J. *A Course in Statistical Mechanics*; Prentice Hall: Englewood Cliffs, NJ, 1985.
(12) Burchard, W. *Macromol. Symp.* **1990**, *39*, 179.
(13) Yamakawa, H. *Modern Theory of Polymer Solutions*; Harper & Row: New York, 1971.
(14) Ioan, C. E.; Aberle, T.; Burchard, W. *Macromolecules* **2000**, *33*, 5730.
(15) Nordmeier, E. *J. Phys. Chem.* **1993**, *21*, 5770.
(16) Siegert, A. J. F. *MIT Rad. Lab. Rep., No. 465*, 1943.
(17) Burchard, W.; Schmidt, M.; Stockmayer, W. H. *Macromolecules* **1980**, *13*, 580, 1265.
(18) Einstein, *A. Ann. Phys.* **1905**, *17*, 549; **1906**, *19*, 371.
(19) Pecora, R. *J. Chem. Phys.* **1964**, *40*, 1604; **1965**, *43*, 1562.
(20) Kohlrausch, R. *Pogg. Ann. Phys. Chem.* **1854**, *91*, 179; **1863**, *119*, 337.
(21) Lindsey, C. P.; Patterson, G. *J. Chem. Phys.* **1980**, *73*, 3348.
(22) De Groot, *Thermodynamik Irreversibler Prozesse*; Bibliographisches Institut: Mannheim, Germany, 1960.
(23) Ioan, C. E.; Aberle, T.; Burchard, W. *Macromolecules* **1999**, *32*, 7444.
(24) Durrani, C. M.; Donald, M. *Carbohydr. Polym.* **2000**, *41*, 207.
(25) Stauffer, D. *Introduction to Percolation Theory*; Taylor and Francis: London, and Philadelphia, PA, 1985.
(26) Stockmayer, W. H. *J. Chem. Phys.* **1943**, *11*, 45; **1944**, *12*, 105.
(27) (a) Auersch, A.; Littke, W.; Lang, P.; Burchard, W. *J. Cryst. Growth* **1991**, *110*, 201. (b) Schulz, L.; Burchard, W. *Papier* **1989**, *43*, 665. (c) Burchard, W.; Lang, P.; Schulz, L.; Coviello, T. *Macromol. Symp.* **1992**, *58*, 28.
(28) Stauffer, D.; Coniglio, A.; Adam, M. *Adv. Polym. Sci.* **1982**, *44*, 105.
(29) Zimm, B. H.; Stockmayer, W. H. *J. Chem. Phys.* **1949**, *17*, 1301.
(30) Carnahan, N. F.; Starling, K. E. *J. Chem. Phys.* **1969**, *51*, 639.
(31) Ohta, T.; Oono, Y. *Phys. Lett.* **1983**, *79*, 339.
(32) Wiltzius, R.; Haller, H. R.; Cannell, D. S.; Schaefer, D. W. *Phys. Rev. Lett.* **1983**, *51*, 1183; **1984**, *53*, 834.
(33) Semenow, A. N.; Rubinstein, M. *Macromolecules* **1998**, *31*, 1373.

MA992060Z